Spatially resolved Eu(III) environments by chemical microscopy

Vogel, M.; Steudtner, R.; Fankhänel, T.; Raff, J.; Drobot, B.;

Originally published:

September 2021

Analyst 146(2021), 6741-6745

DOI: https://doi.org/10.1039/D1AN01449H

COMMUNICATION

Spatially resolved Eu(III) environments by chemical microscopy.

Manja Vogel, [a] Robin Steudtner, [b] Johannes Raff [b] and Björn Drobot *[b]

Received 00th January 20xx,
Accepted 00th January 20xx

DOI: 10.1039/x0xx00000x

Chemical microscopy combines high-resolution emission spectra with Abbe-limited spatial resolution and is used for studies of inhomogeneous samples at the nanoscale. The spatial distinction of multiple Eu(III) coordination sites allows for a comprehensive understanding of environmental samples and highlights the applicability of Eu(III) as molecular probe in medicine and biology.

The local identification and characterization of molecular structures in various geological and biological systems plays an important role in all areas of environmental science. The range of methods for determining spatial resolution in the sub-micron range is manifold and reaches from A for atomic force microscopy (AFM) to Z for Z-STEM (atomic number contrast scanning transmission electron microscopy). Each microscopy technique has its own requirements – e.g., vacuum or atmosphere, hydrate or water free, fixed samples or native, and non-destructive or destructive – which could interfere with the sample or the target molecule. In environmental science, the localization and transport of (heavy metal) ions and their chemical form (speciation) is of particular importance. The application of imaging techniques such as electron microscopy (scanning or transmission), nano-secondary ion mass spectrometry (NanoSIMS), X-ray based microscopy, emission lifetime imaging (FLIM/PLIM), or hyperspectral imaging techniques have all clearly expanded over the last 20 years [1-5]. Nonetheless, the direct determination of metal speciation using these techniques remains quite challenging. Energy dispersive X-ray analysis (EDXA) of electron microscopic pictures is useful for providing the elementary composition of each sample point. Based on the detection limit, which ranges between 0.1 and 10 wt% [6], major and minor elements can be determined in one measurement. However, the resulting elemental spectrum can feature overlapping peaks; in such instances, interpreting the automated identification of peaks often demands the additional skill and experience of the user [7]. This challenge can be amplified in the case of biological samples with their ubiquitous presence of carbon, nitrogen, and phosphorus, thus further complicating the species-specific analysis of the metals. In contrast, NanoSIMS simplifies the task of studying biological processes at the single cell or subcellular level [8]. By applying this approach for mapping a biological sample, the distribution of various elements can be localized and quantified at the cellular or intracellular level with a local resolution down to 50 nm. Although the sensitivity of this method is one order of magnitude lower (ppb level) compared to energy dispersive X-ray analysis, the sample preparation is similarly challenging.

Spatially resolved X-ray absorption spectroscopy with the X-ray absorption near edge structure (XANES) and extended X-ray absorption fine structure (EXAFS) analysis provides information about the element oxidation state and the composition of the first coordination sphere. However, distinguishing between the different complexes of a target element that are present in parallel is challenging due to the superposition of their signals. A comparison of different X-ray mapping techniques with respect to excitation source, element specificity, modalities, analytical depth, spatial resolution, limits of detection, measurement conditions and sample preparation was published by van der Ent et al. [5]. Another approach for mapping biological or geological samples is (confocal) microscopy with inorganic or organic fluorophores after excitation with UV or visible light. Here also, the range of possible applications extends from the simple assignment of primary colors (red, green, blue) to a full spectral resolved fluorescence spectrum for each pixel via the use of hyperspectral imaging techniques. Importantly, the proper fluorophore must be used to study the local area of interest (biological/geological). Although organic fluorophores are typically used as light-emitting substances, recent advances successfully employed lanthanide-based optical probes in various biological systems [9]. In particular, the unique luminescent properties of lanthanides (Ln) are based on

[a] *HZDR Innovation GmbH, Bautzner Landstraße 400, 01328 Dresden, Germany*
[b] *Helmholtz-Zentrum Dresden-Rossendorf e.V., Institute of Resource Ecology, Bautzner Landstraße 400, 01328 Dresden, Germany*

Electronic Supplementary Information (ESI) available: Experimental details, microscopic and laser spectroscopic setup, XRD and luminescence data. See DOI: 10.1039/x0xx00000x

parity-forbidden transitions involving the 4*f* atomic orbitals. In general, the lanthanide luminescence emission (peak position) is unaffected by the chemical environment; only a change in luminescence lifetime will be observed due to the exchange of water molecules in the first coordination sphere. This effect can be used for lifetime imaging, where the image contrast is generated by the emission lifetime of the emitter. In the case of lanthanides/actinides the luminescence decay is long (in the order of milli seconds) compared to organic fluorophores (in the order of pico seconds). The lower decay requires increased pixel dwell times, which in turn will increase the PLIM image acquisition time compared to the FLIM image acquisition time by several orders of magnitude. In addition, the simultaneous occurrence of several different metal environments results in superposed decay curves, which are hard to interpret.

Trivalent europium (Eu(III)) is the exception in the lanthanide series. The fine structure of individual transitions in the emission spectrum (further details in SI – Figure S 1) and their intensities are sensitive to different chemical environments. Therefore, Eu(III) can be used as a luminescent probe to study the coordination sphere in various biological and geological systems. Since Ln(III) feature ionic radii similar to calcium(II) ions, they have often been used as analogues to study binding sites, signaling or transport pathways, or lewis acid-activated mechanisms [10-12]. In addition to their use as luminescent probes, lanthanides are frequently used as nonradioactive analogs for the trivalent actinides (An) in environmental sciences.

Given the environmental complexity associated with a wide variety of chemical microenvironments that influence the behavior of lanthanides, the presence of a single Ln species is unlikely in such systems. Accordingly, we present chemical microscopy — a combination of microscopy with high resolution luminescence spectroscopy — in order to provide new insights into the spatial distribution of Eu(III) species under various ambient conditions. To verify the performance of the used micro-spectroscopic setup, we initially benchmarked four distinct Eu(III)-containing compounds — Eu_2O_3, $Eu_2(oxalate)_3$, $NaEu(SO_4)_2 \cdot H_2O$ and $EuPO_4$ — first individually and then as a mixture (further details are described in SI). Luminescence spectroscopic mapping of these Eu(III) species was carried out with a Raman microscope using a 532 nm laser for excitation. Acquisition and basic treatment of data was performed with LabSpec 5 software (Horiba Jobin Yvon) and OriginPro 2019. Figure 1 (right side) provides a light-microscopic image of the mixed-powder sample. In the next step, a specific region of interest was mapped spectroscopically in both horizontal and vertical orientations. The resulting luminescence light was collected in the wavelength range from 570 to 715 nm. All spectra were background corrected using a self-implemented version of a 'rolling ball' algorithm [13]. Data deconvolution was performed by an iterative factor analysis (N-way toolbox for Matlab [14]) using randomized initial guesses. To account for physical data, the spectra of the factors and distributions were restricted to being non-negative (NIFA – non-negative iterative factor analysis).

Figure 1 (left side) provides the luminescence spectra for each of the four Eu(III) compounds, along with a comparison of the pure compound spectra (top green, separate measure) and the deconvoluted spectra from NIFA (bottom orange). Although excitation at 532 nm in the rare $^7F_1 \rightarrow {}^5D_1$ transition was used [15], the spectra were well-resolved and represent all the main luminescence bands of the transition from $^5D_0 \rightarrow {}^7F_0$ to $^5D_0 \rightarrow {}^7F_4$. Based on the special spectral characteristics of the four spectra derived from NIFA, we were able to achieve unambiguous assignment to the spectra of the pure components using this proof of concept. Both spectra, pure and deconvoluted, are almost identical. Their absolute intensities of the $^5D_0 \rightarrow {}^7F_0$ transitions, their intensity ratios of the transitions $^5D_0 \rightarrow {}^7F_2$ and $^5D_0 \rightarrow {}^7F_1$ (F_2/F_1), and the crystal-field splitting of each transition from $^5D_0 \rightarrow {}^7F_0$ to $^5D_0 \rightarrow {}^7F_4$, match perfectly. These results clearly demonstrate the applicability of the

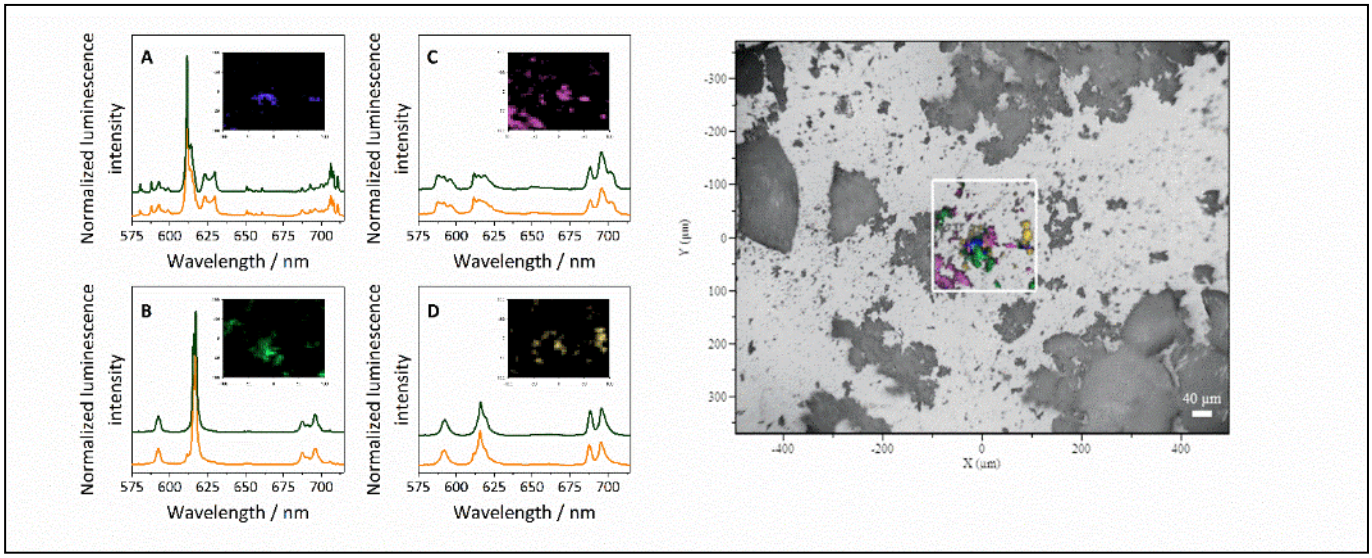

Figure 1: Left – Single component luminescence spectra of the pure measured compound (green) in comparison to the deconvoluted spectra analysed by NIFA (orange) for A) Eu_2O_3 B) $Eu_2(oxalate)_3$ C) $EuPO_4$ D) $NaEu(SO_4)_2 \cdot H_2O$ with the corresponding local distribution (inset). Right – Microscopic image of mixed powder sample with the region of interest (white square) and the overlay of the spectroscopic mapping analyses. objective: 10fold magnification (laser spot size of ca. 2.6 µm), Λexc. = 532 nm, exposure time 1 s, ROI 200x200 µm, step size of 5 µm in horizontal and vertical orientation.

employed microscopic system for the chemical microscopy analysis of environmental samples. The disadvantage of the low direct signal-to-structure assignment capability in Eu(III) luminescence spectroscopy can be overcome by comparison with known spectra, either self-measured or from a database. The corresponding local species distribution for the ROI was derived using NIFA as described above for the 2601 single points. Figure 1 A-D provides mapping results for the individual Eu(III) compounds, which were overlaid in the ROI of the light-microscopic image (white frame).

After successful setup validation with the artificial system, a ternary system consisting of Eu(III), calcite, and *Shewanella oneidensis* MR-1 was investigated. This system, which represents more realistic imitation of a natural sample, was utilized to confirm the general applicability of the chemical microscopy setup toward various biological and geological systems. This complex interaction is an extension of the Eu(III)-calcite, Eu(III)-*Shewanella oneidensis* MR-1, and calcite-*Shewanella oneidensis* MR-1 binary systems previously studied. The Eu(III)-calcite-system was intensively studied using different spectroscopic and microscopic techniques [16-19]. As documented in these prior studies, three different Eu(III)-calcite species were described. The association of Eu(III) with Gram-negative bacteria (for example, *Shewanella* belongs to this class) features rapid biosorption; in this case the Eu(III) is largely sorbed extracellularly by binding sites located within the cell wall structure [20, 21]. Furthermore, it was shown that *Shewanella oneidensis* MR-1 affected the mineral surface of calcite [22]. Under aerobic conditions, carbonate dissolution was influenced by two distinct mechanistic pathways: etch pit development and the excavation of carbonate material at the cell–mineral interface during the irreversible attachment of *Shewanella oneidensis* MR-1.

We then investigated the role of Eu(III) in the dynamic and competitive relationship between bioassociation at the microbial surface and sorption on calcite as representative component for natural environments. A knapped flint calcite was incubated with *Shewanella oneidensis* MR-1 in order to grow a biofilm on the mineral surface, as published by Davies et al. [22] After two days the microbial afflicted crystal was transferred into an Eu(III)-containing solution for one day. Prior to conducting luminescence spectroscopic mapping, both the slightly bound Eu(III) and salt were removed from the crystal by washing with deionized water. The successful colonization by the rod-shaped bacteria is clearly visible in Figure 2 (inset – right side). The typically rod shape (2-3 µm in length, 0.4-0.7 µm in diameter) of single *Shewanella oneidensis* MR-1 cells, coupled with the formation of the biofilm, can be seen. The subsequent deconvolution of luminescence spectroscopic mapping data with NIFA provided three signal sets: one Raman and two emission spectra. The overlay of the local distribution with the microscopic image facilitated a detailed description of the three components. As shown in Figure 2, the *Shewanella oneidensis* MR-1 biofilm covers about 50% of the calcite surface; moreover,

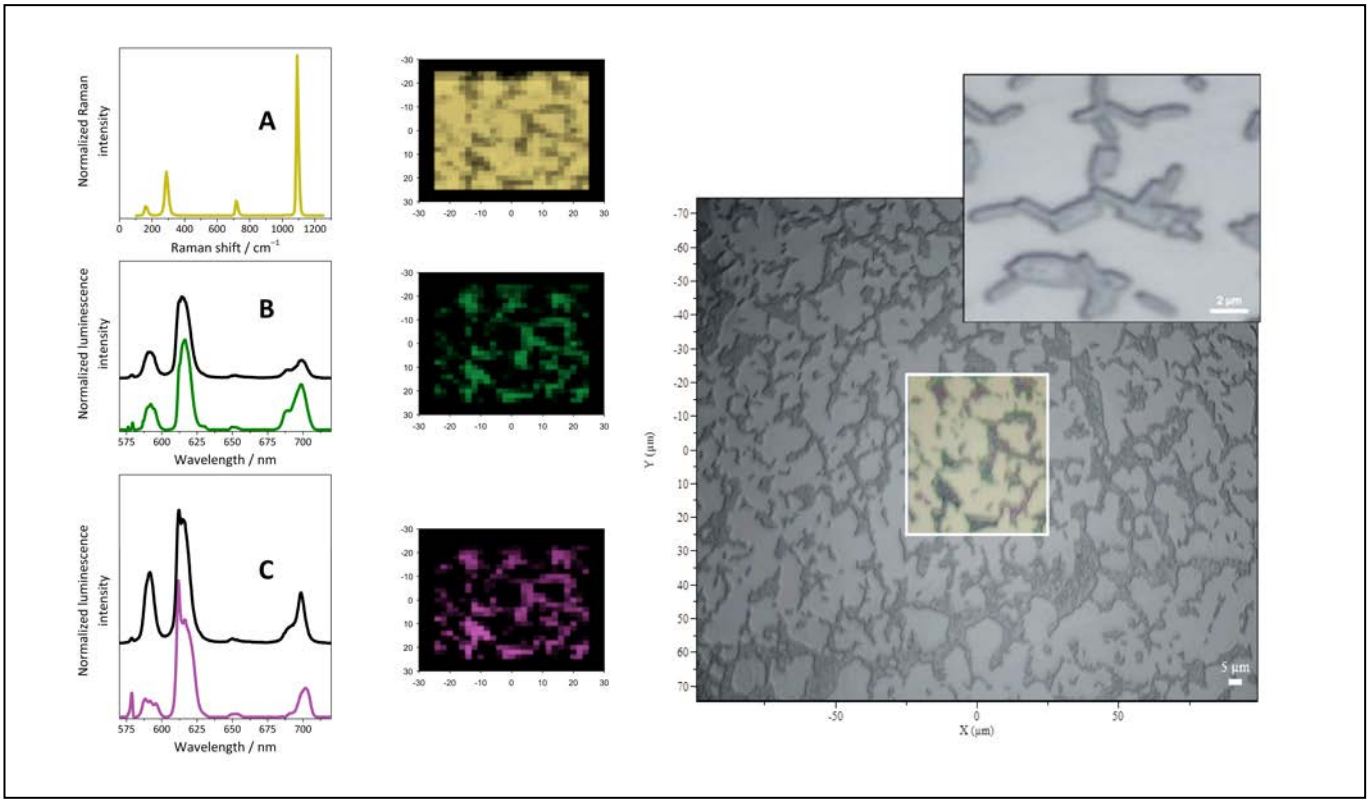

Figure 2: Left – A) Deconvoluted Raman spectrum of calcite; B & C) Comparison of the deconvoluted luminescence spectra obtained by TRLFS (black) and by mapping (coloured) for Eu(III) bound to protein-like structures (B) and Eu(III) complexed with biofilm eDNA (C); Middle – corresponding local distribution of calcite and biofilm associated Eu(III) species. Right – Microscopic image of Eu(III)-calcite-*Shewanella oneidensis* MR-1 sample with the region of interest (white square) and overlay of the spectroscopic mapping analyses. Additionally, a zoom-in of microscopic image of single *Shewanella oneidensis* MR-1 cells. objective: 50-fold magnification (laser spot size of ca. 0.9 µm), $\Lambda_{exc.}$ = 532 nm, exposure time 10 s, ROI 25x25 µm, step size of 2 µm in horizontal and vertical orientation.

the omnipresent yellow NIFA component is the only signal for the pure calcite regions and corresponds to the Raman spectrum (Figure 2 A). Note that the spectrum consists of four characteristic peaks at 162, 288, 717 and 1091 cm^{-1}, which agree with literature data for calcite. The main peaks at 1091 cm^{-1} and 717 $cm^{-1}$are assigned to the A_g internal mode that derives from the v_1 symmetric stretching mode, and the v_4 of the in-plane bending mode of the carbonate ion, respectively [23]. The two additional peaks at 162 and 288 cm^{-1} correspond to the translational and rotational lattice modes of CO_3^{2-}. The remaining two NIFA components (green and magenta, Figure 2 B, C) represent typical Eu(III) emission spectra. Both components overlay exclusively with image regions where *Shewanella* oneidensis MR-1 cells are present. These findings suggest that Eu(III) bioassociation is preferred over mineral sorption to calcite. Moreover, the two different Eu(III) species are homogeneously distributed across the biofilm of *Shewanella oneidensis* MR-1. The F_2/F_1 ratio was found to be 3.5 for species B and 6.0 for species C. An interesting feature of species C is the prominent shoulder in the F_2 transition. To better understand the results from luminescence mapping, a sample of *Shewanella oneidensis* MR-1 cell incubated with Eu(III) was prepared. After one day the cells were washed and analyzed by time-resolved laser-induced fluorescence spectroscopy (TRLFS) using an excitation wavelength of 394 nm, which is the common excitation wavelength for Eu(III). Parallel factor analysis (PARAFAC [24]) was used for bulk data decomposition, as described elsewhere. Based on their spectral characteristics, the two deconvoluted TRLFS Eu(III) species (black spectra in Figure 2 B, C) were assigned to the two Eu(III) species obtained via chemical microscopy. Additionally, luminescence lifetimes (τ) were extracted from TRLFS as follows: 395 µs for species B and 174 µs for species C. To identify the *Shewanella oneidensis* MR-1 biofilm associated with the Eu(III) species, one must consider typical extrapolymeric substances (EPS) like polysaccharides, proteins, glycoproteins, and glycolipids, and in some cases, amazing amounts of extracellular DNA (eDNA) [25]. Additionally, it is known that the formation of a *Shewanella oneidensis* MR-1 biofilm strongly depends on (eDNA) as a structural component. In contrast, in the absence of eDNA, *Shewanella oneidensis* MR-1 cells are severely reduced in surface adhesion and subsequent formation of three-dimensional structures [26, 27]. In addition to its structural and/or adhesive role in biofilms, eDNA was demonstrated to chelate cations required for stabilizing lipopolysaccharides and/or outer membranes, thereby causing antimicrobial activity [28]. On that basis, we compared the special spectral characteristics of the Eu(III) species C with literature data for DNA origami nanostructures with Eu(III) coordination [29] and a complementary Eu(III) study in the presence of nucleic acid (supporting information). The congruence of the spectral characteristics was found to be perfect; all features (F_2/F_1 ratio, τ and the shoulder in F_2 band) were found to be nearly identical. Therefore, we assigned the chemical microscopy species C to a Eu(III) complexed with biofilm eDNA excreted by the *Shewanella oneidensis* MR-1 cells. It should be noted that while the luminescence data of the second Eu(III) species (Figure 2 B) did not evidence any characteristic spectral features, the F_2/F_1 ratio changed and the luminescence lifetime increased in comparison to both the free Eu(III) aquo ion and the Eu(III) complexed with biofilm eDNA. Extended luminescence lifetimes are commonly associated with the displacement of water molecules from the metal coordination sphere. Thus, this Eu(III) binding site is highly coordinated and shields the Eu(III) against the aqueous surrounding. Proteinaceous structures such as high-affinity calcium binding sites can provide such an environment. A direct spectroscopic comparison with Eu(III) associated to a specific protein from *Shewanella oneidensis* MR-1 cells is not yet possible given the sizable number of proteins in *Shewanella oneidensis* MR-1 that might contribute to this interaction. Therefore, further biological work-up processes are suggested for further studies of these systems. Nevertheless, a comparison of the spectral features (F_2/F_1 ratio, τ and shape of the F_4 band) with Eu(III) bound to other protein structures (α-amylase [30], calmodulin [24]) suggests a protein bonded Eu(III) as our second species (species B).

Summarizing, we successfully applied chemical microscopy to two different Eu(III) systems. In our first proof-of-concept assay, we investigated a four-component mixed-powder sample and identified and visualized the individual Eu(III) components. Notably, their spectral features correspond well with reference data and clearly show the strength of our developed workflow. In a second experiment, we highlighted the spatial distinction of multiple Eu(III) coordination sites in the ternary Eu(III) – calcite - *Shewanella oneidensis* MR-1 system. The results described herein suggest a new field of analysis for investigating complex interaction processes in environmental systems. Overall, this chemical microscopy study demonstrates the high potential of non-functionalized Eu(III) as a molecular probe, ultimately contributing to a comprehensive understanding (localization, identification and chemical characterization) of Ln/An interaction pathways and their migration in our environment.

We argue that chemical microscopy will benefit significantly from the planned implementation of a tuneable laser for narrow linewidth excitation scans, which will expand the portfolio of luminescent targets and enable the analysis of even more complex systems. Additionally, a correlation of chemical microscopy with other techniques, e.g., AFM, can provide supplementary information that will further enhance our understanding of complex bio-systems.

Conflicts of interest

There are no conflicts to declare.

Acknowledgements

The authors sincerely thank Sindy Kluge for her assistance with the Eu(III) calcite *Shewanella oneidensis* MR-1 experiments. We also acknowledge Salim Shams and Stephan Weiss for their characterization of the Eu(III) powders by X-ray diffraction; and Tobias Fankhänel for his contributions in preparing and measuring the Eu(III) RNA titration series with TRLFS.

Notes and references

1. K. L. Moore, E. Lombi, F.-J. Zhao and C. R. M. Grovenor, *Analytical and Bioanalytical Chemistry*, 2012, **402**, 3263-3273.
2. F.-J. Zhao, K. L. Moore, E. Lombi and Y.-G. Zhu, *Trends in Plant Science*, 2014, **19**, 183-192.
3. E. Malucelli, M. Fratini, A. Notargiacomo, A. Gianoncelli, L. Merolle, A. Sargenti, C. Cappadone, G. Farruggia, S. Lagomarsino and S. Iotti, *Analyst*, 2016, **141**, 5221-5235.
4. P. M. Kopittke, T. Punshon, D. J. Paterson, R. V. Tappero, P. Wang, F. P. C. Blamey, A. van der Ent and E. Lombi, *Plant Physiol*, 2018, **178**, 507-523.
5. A. van der Ent, W. J. Przybylowicz, M. D. de Jonge, H. H. Harris, C. G. Ryan, G. Tylko, D. J. Paterson, A. D. Barnabas, P. M. Kopittke and J. Mesjasz-Przybylowicz, *New Phytologist*, 2018, **218**, 432-452.
6. S. Nasrazadani and S. Hassani, in *Handbook of Materials Failure Analysis with Case Studies from the Oil and Gas Industry*, eds. A. S. H. Makhlouf and M. Aliofkhazraei, Butterworth-Heinemann, 2016, DOI: https://doi.org/10.1016/B978-0-08-100117-2.00010-8, pp. 39-54.
7. S. P. Lynch, in *Gaseous Hydrogen Embrittlement of Materials in Energy Technologies*, eds. R. P. Gangloff and B. P. Somerday, Woodhead Publishing, 2012, vol. 2, pp. 274-346.
8. F. Gyngard and M. L. Steinhauser, *Journal of Analytical Atomic Spectrometry*, 2019, **34**, 1534-1545.
9. U. Cho and J. K. Chen, *Cell Chemical Biology*, 2020, **27**, 921-936.
10. E. E. Snyder, B. W. Buoscio and J. J. Falke, *Biochemistry*, 1990, **29**, 3937-3943.
11. J. Wojcik, J. Goral, K. Pawlowski and A. Bierzynski, *Biochemistry*, 1997, **36**, 680-687.
12. S. Lim and S. J. Franklin, *Cellular and Molecular Life Sciences CMLS*, 2004, **61**, 2184-2188.
13. S. R. Sternberg, Berlin, Heidelberg, 1982.
14. C. A. Andersson and R. Bro, *Chemometrics and Intelligent Laboratory Systems*, 2000, **52**, 1-4.
15. K. Binnemans, *Coordination Chemistry Reviews*, 2015, **295**, 1-45.
16. T. Stumpf, H. Curtius, C. Walther, K. Dardenne, K. Ufer and T. Fanghänel, *Environ. Sci. Technol.*, 2007, **41**, 3186-3191.
17. M. Marques Fernandes, M. Schmidt, T. Stumpf, C. Walther, D. Bosbach, R. Klenze and T. Fanghänel, *J. Colloid Interface Sci.*, 2008, **321**, 323-331.
18. M. Schmidt, T. Stumpf, M. Marques Fernandes, C. Walther and T. Fanghänel, *Angewandte Chemie-International Edition*, 2008, **47**, 5846-5850.
19. S. Hofmann, K. Voitchovsky, M. Schmidt and T. Stumpf, *Geochim. Cosmochim. Acta*, 2014, **125**, 528-538.
20. T. Ozaki, T. Ohnuki, T. Kimura and A. J. Francis, *Journal of Nuclear and Radiochemical Sciences*, 2005, **6**, 73-76.
21. A. C. Texier, Y. Andres, M. Illemassene and P. Le Cloirec, *Environ. Sci. Technol.*, 2000, **34**, 610-615.
22. K. J. Davis, K. H. Nealson and A. Luttge, *Geobiology*, 2007, **5**, 191-205.
23. F. C. Donnelly, F. Purcell-Milton, V. Framont, O. Cleary, P. W. Dunne and Y. K. Gun'ko, *Chem. Commun.*, 2017, **53**, 6657-6660.
24. B. Drobot, M. Schmidt, Y. Mochizuki, T. Abe, K. Okuwaki, F. Brulfert, S. Falke, S. A. Samsonov, Y. Komeiji, C. Betzel, T. Stumpf, J. Raff and S. Tsushima, *Physical Chemistry Chemical Physics*, 2019, **21**, 21213-21222.
25. H. C. Flemming, T. R. Neu and D. J. Wozniak, *Journal of Bacteriology*, 2007, **189**, 7945-7947.
26. J. Gödeke, K. Paul, J. Lassak and K. M. Thormann, *Isme Journal*, 2011, **5**, 613-626.
27. J. Gödeke, M. Heun, S. Bubendorfer, K. Paul and K. M. Thormann, *Applied and Environmental Microbiology*, 2011, **77**, 5342-5351.
28. H. Mulcahy, L. Charron-Mazenod and S. Lewenza, *Plos Pathogens*, 2008, **4**.
29. L. Opherden, J. Oertel, A. Barkleit, K. Fahmy and A. Keller, *Langmuir*, 2014, **30**, 8152-8159.
30. A. Barkleit, A. Heller, A. Ikeda-Ohno and G. Bernhard, *Dalton Transactions*, 2016, **45**, 8724-8733.

‡ Footnotes relating to the main text should appear here. These might include comments relevant to but not central to the matter under discussion, limited experimental and spectral data, and crystallographic data.